frontiers in Physics

BRIEF RESEARCH REPORT
published: 10 January 2022
doi: 10.3389/fphy.2021.810220

Oxygen Hole Character and Lateral Homogeneity in $PrNiO_{2+\delta}$ Thin Films

*K. Fürsich[1], R. Pons[1], M. Bluschke[1], R. A. Ortiz[1], S. Wintz[2], E. Schierle[3], M. Weigand[3], G. Logvenov[1], G. Schütz[2], B. Keimer[1] and E. Benckiser[1]**

[1]Max Planck Institute for Solid State Research, Stuttgart, Germany, [2]Max Planck Institute for Intelligent Systems, Stuttgart, Germany, [3]Helmholtz-Zentrum Berlin für Materialien und Energie, Berlin, Germany

Using x-ray absorption spectroscopy with lateral resolution from the submillimeter to submicrometer range, we investigate the homogeneity, the chemical composition, and the nickel 3*d*- oxygen 2*p* charge transfer in topotactically reduced epitaxial $PrNiO_{2+\delta}$ thin films. To this end, we use x-ray absorption spectroscopy in a standard experimental setup and in a soft x-ray microscope to probe the element and spatially resolved electronic structure modifications through changes of the nickel-2*p* and oxygen-1*s* absorption spectrum upon soft-chemistry reduction. We find that the reduction process is laterally homogeneous across a partially reduced $PrNiO_{2+\delta}$ thin film sample for length scales down to 50 nm.

Keywords: infinite-layer nickelates, x-ray absorption spectroscopy, x-ray microscopy, topotactical soft chemistry reduction, rare-earth nickelates films

OPEN ACCESS

Edited by:
Danfeng Li,
City University of Hong Kong, Hong Kong SAR, China

Reviewed by:
Motoki Osada,
Stanford University, United States
Atsushi Fujimori,
The University of Tokyo, Japan
Zhihai Zhu,
Institute of Physics (CAS), China

****Correspondence:***
E. Benckiser
E.Benckiser@fkf.mpg.de

Specialty section:
This article was submitted to Condensed Matter Physics, a section of the journal Frontiers in Physics

Received: *06 November 2021*
Accepted: *08 December 2021*
Published: *10 January 2022*

Citation:
Fürsich K, Pons R, Bluschke M, Ortiz RA, Wintz S, Schierle E, Weigand M, Logvenov G, Schütz G, Keimer B and Benckiser E (2022) Oxygen Hole Character and Lateral Homogeneity in $PrNiO_{2+\delta}$ Thin Films. Front. Phys. 9:810220. doi: 10.3389/fphy.2021.810220

1 INTRODUCTION

Although theoretically considered already decades ago [1], superconductivity in nickelates with infinite-layer structure was only realized recently [2]. In particular, Sr and Ca-doped rare-earth nickelate thin films with composition $RNiO_2$ (R = La, Pr, Nd) show a superconducting transition below 9–15 K [3–6]. This discovery triggered a lot of research activity that uncovered similarities [1, 7], but also significant differences [8, 9] between nickelates and cuprates. It remains to be seen whether it is the similarity or the difference that will contribute to our understanding of unconventional superconductivity. Before that, however, many questions about these superconducting nickelates still have to be answered. These concern in particular the role of heteroepitaxy with the underlying substrate, the exact chemical composition and crystal structure as well as the homogeneity of the distribution of the dopant ions and the oxygen removal.

To date superconductivity in nickelates has only been realized in epitaxially stabilized thin films, including the related, topotactically-reduced Ruddlesden-Popper compounds [10]. Such heterostructures are a challenge for standard characterization tools such as neutron scattering due to their small sample mass. Hence, x-ray absorption (XAS) and resonant x-ray scattering studies provided significant insights into the ground state and electronic structure of infinite-layer nickelates, and therefore serve as important experimental probes to compare nickelates and cuprates.

XAS and resonant inelastic x-ray scattering (RIXS) at Ni-L edge energies revealed a doping dependent electronic structure of infinite-layer nickelates and indicate a d^8 spin-singlet ground state, where the doped holes occupy the $d_{x^2-y^2}$ orbitals in analogy to single-band Hubbard models [11]. A high-resolution RIXS study identified spin excitations in infinite-layer nickelates with a bandwidth of 200 meV [12], which can be explained in terms of dynamical correlations giving rise to large antiferromagnetic nearest-neighbor exchange interactions [13]. Along these lines, several studies point towards the importance of the itinerant electrons from the rare-earth ions, and their hybridization with the Ni d states, in particular for the exchange coupling, and for

superconductivity in general [14]. Further XAS studies at the Ni-*L* edge focused on the Ni-O hybridization and found that the hybridization can be modulated by the film thickness [6].

Due to the hybridization between Ni-3*d* and O-2*p* states, XAS at the O-*K* edge serves as another independent characterization tool in transition metal oxides. In particular, O-*K* edge XAS measurements revealed a prominent pre-peak, indicative of the strong $3d - 2p$ hybridization between nickel and oxygen, and the negative charge-transfer character of perovskite $RNiO_3$. Since this feature is indiscernible in infinite-layer $RNiO_2$ [14, 15, 11, 16], the well-isolated pre-peak (usually at around 528 eV) serves as a reliable characteristic to track the state of reduction of the sample under investigation. In addition, the absence of strong Ni-O hybridization in infinite-layer nickelates suggests a clear difference to superconducting cuprates with strong Cu-O hybridization [17]. A recent scanning-transmission electron microscopy (STEM) and electron energy loss spectroscopy (EELS) study on infinite-layer nickelate thin films reported that with increasing hole-doping an additional spectral weight emerges at around 529 eV, which is imposed on the rising edge of the O-*K* edge [15]. This feature is attributed to $d^9\,\underline{L}$ states, where $\underline{L}$ represents a hole residing on the oxygen ligands. This phenomenology is reminiscent of hole-doped cuprates, where the Zhang-Rice singlet arises when holes are doped into the CuO_2 planes.

The above studies have given important insights into the phase behavior in rare-earth nickelates and the topotactic stabilization of the infinite layer phase. While this soft-chemistry synthesis of the infinite-layer phase with different rare-earth elements and/or doping levels has already been extensively dealt with in several studies, information on the lateral, spatial distribution of oxygen content and Ni valence state has so far been little investigated. Since superconductivity was only observed in epitaxial thin layers, the question arises to what extent the reduction process is sample-specific here. In particular, lattice defects resulting from the lattice mismatch with the substrate, spatially varying cation stoichiometry as a result of the growth process, and islands resulting from mixed layer-by-layer and island growth typical of these nickelate layers, are areas where an inhomogeneous reduction can occur. Therefore, spatially resolved information about the oxidation state and the oxygen de-intercalation pathways in these compounds may reveal strategies for enhancing superconductivity in the nickelates.

Here we present results from XAS, measured in total-electron yield in a standard setup and in an x-ray microscope, to study spatial variations of the Ni valence state and oxygen stoichiometry in reduced nickelates over a large lateral scale. We observe high homogeneity down to a lateral length scale of ~ 50 nm.

2 METHODS

The investigated sample is a 15 nm-thick $PrNiO_3$ film on (110)-oriented $NdGaO_3$ that was grown by ozone-assisted atomic layer-by-layer molecular beam epitaxy (MBE). The growth was performed by sequentially opening the Pr and Ni effusion cells under an ozone atmosphere of 2.4×10^{-5} mbar, while the substrate was heated to about 600°C. Before growth, the effusion cell evaporation rates were determined in vacuum using a quartz crystal microbalance. The rates were then constantly adjusted during growth according to the reflection high-energy electron diffraction (RHEED) feedback. The as-grown sample was cut in several pieces, where one piece was kept pristine, while the others were topotactically reduced. We used CaH_2 as the reduction agent, which was physically separated from the sample in an evacuated quartz glass ampoule and heated at 250 °C for 12 h (not including the 30 min to ramp our oven up from room temperature), following previously established protocols [16, 18, 2].

All samples were characterized by in-house hard x-ray diffraction to track changes in the out-of-plane lattice constant *c* upon reduction (see **Figure 1**). For the pristine perovskite $PrNiO_3$ sample we find $c = 3.79\,\mathring{A}$, slightly smaller than the bulk value due to moderate tensile strain imposed by the $NdGaO_3$ substrate. Upon reduction, the out-of-plane lattice spacing is substantially reduced corresponding to a value of $c = 3.62\,\mathring{A}$, which is larger than $c = 3.31\,\mathring{A}$ reported for $PrNiO_2$ grown on $SrTiO_3$ in Ref. [5]. This deviation results from a combination of the different lattice mismatch with the substrates and an incomplete transition to the infinite-layer phase. Corroborated by our O-*K* edge XAS measurements and the comparison to literature we estimate the stoichiometry of our film to be close to $PrNiO_{2.3}$ [19–21]. We take advantage of this and use the partially reduced nickelate film to examine possible oxygen inhomogeneities and/or identify possibly non-reduced areas.

We used both endstations of the UE46 beamline of BESSY II at the Helmholtz-Zentrum Berlin. XAS measurements over a large sample area were carried out in the XUV diffractometer at UE46-PGM1, while we used the x-ray microscope (UE46-MAXYMUS endstation) [22] to map out the chemical composition and electronic structure with up to four orders of magnitude higher spatial resolution. For the standard XAS measurements the footprint of the beam on the sample was approximately 250 µm × 200 µm, while the energy-dependent XAS measurements at MAXYMUS were performed with a beam diameter of ≈ 5 µm ("defocused beam"). For the spatially resolved image maps at fixed energies, we further decreased the beam footprint to facilitate a spatial resolution of 50 nm. All XAS measurements were performed at room temperature with horizontally polarized light at normal incidence $\theta = 90^\circ$ and in total-electron yield (TEY) mode. The probing depth in our measurements is limited by the electron escape depth, which is below 10 nm (approximately one third of our sample thickness) for energies of relevance here.

All spectra taken across the Ni-*L* edge are normalized to the post-edge region (around 876 eV), whereas the data measured across the O-*K* edge were normalized to the value at 536 eV. To facilitate a comparison between energy and image scans, we normalized the image scans to the exposure time and the number of photons (among others determined by the opening of the exit slits).

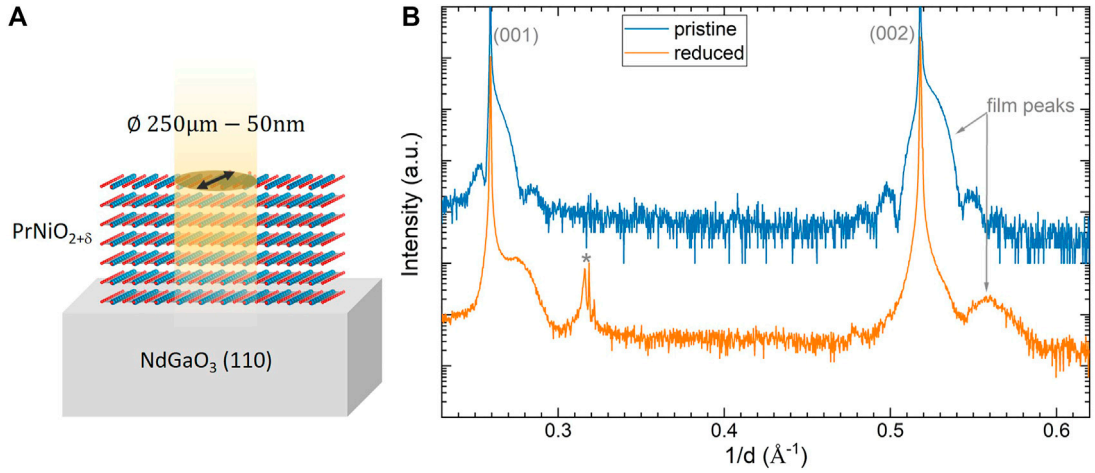

FIGURE 1 | (A) Sketch of the $PrNiO_{2+\delta}$ thin film on a $NdGaO_3$ substrate, indicating the large variation of the soft x-ray beam diameter used to investigate its lateral chemical homogeneity. **(B)** Hard x-ray diffraction around the (001) and (002) $NdGaO_3$ substrate reflection for the pristine (blue) and the 12 h at 250°C reduced (orange) sample. The film peaks close to the (002) substrate peak are indicated and the star marks a peak arising from the sample holder.

3 RESULTS

3.1 X-Ray Absorption Spectroscopy

Figure 2A shows the XAS measurements taken in the standard experimental setup at the Ni-*L* edge for both pristine and reduced pieces of the same sample. For the pristine piece, we observe the well-known double-peak structure at the Ni-L_3 edge, indicative of charge fluctuations in the metallic phase [23–25]. Upon topotactical reduction, both the Ni-L_2 and L_3 edges shift towards lower energies, suggesting the transition from a Ni^{3+} oxidation state towards Ni^{2+} and Ni^{1+} [11]. We note that these energy shifts imprint also changes of the crystal/ligand field, since the pristine sample has a perovskite structure, whereas the reduced sample adopts an infinite-layer phase, in which apical oxygen ions are successively removed [4, 16]. Without analyzing further details of the spectral features, we consider the difference spectrum, as it clearly reflects the essential changes upon reduction. We observe an increase in spectral weight at lower energies, which at the L_3 edge, is maximal at E_A and is associated with a loss of weight at higher energy, labeled E_B in **Figure 2**. A previous study on $SmNiO_x$ films showed that similar changes in the XAS were already observed between non-stoichiometric $SmNiO_{2.92}$ and $SmNiO_{2.63}$ [19]. From the comparison with this data, we estimate the oxygen stoichiometry of our film to be around 2.3, i.e. already relatively close to the desired stoichiometry, but with the option of testing the lateral homogeneity of the distribution of the remaining 0.3 oxygen ions per formula unit and thus evaluating the reduction process.

To get a first impression on the spatial homogeneity of the reduction process, we next investigate the very same samples by XAS measurements with a much smaller beam footprint [≈ 5µm available at the x-ray microscope, *i.e.* a factor of 50 smaller compared to data in **Figure 2A**. **Figure 2B** shows these XAS measurements at the Ni-*L* edge for both, pristine and reduced sample pieces. The data agrees well with the XAS measurements on the respective pieces with the much larger beam (≈ 250µm, see **Figure 2A**). This indicates already that the Ni oxidation state and consequently the oxygen stoichiometry of the reduced sample is spatially homogeneous at the µm length scale.

We repeat the same measurements for pristine and reduced samples with the small and large beam sizes at the O-*K* edge. **Figure 3** panels A and B show XAS measurements with a beamsize of ≈ 250µm and 5 µm, respectively. As was the case at the Ni-*L* edge, the two spectra taken with different beam sizes resemble each other closely. In particular, we identify the following features: A rather sharp prepeak with the spectral weight centered around 528 eV ("pre-peak") vanished upon reduction in agreement with previous studies [14, 15]. Additionally, we observe an increase in the spectral weight upon reduction in a broad range between 531 eV and 534 eV. Previous studies on Sr-doped $LaNiO_2$ [15] and self-doped $La_4Ni_3O_8$ [21] have associated emerging spectral weight below 531 eV as a contribution reminiscent of the Zhang-Rice singlet in hole-doped cuprates. The increase in the spectral weight we observe here is clearly higher in energy. In cuprates it is possible to adjust the doping required for superconductivity via the oxygen content. Similarly, one would also expect this to be possible for the nickelates. According to our estimation, we expect a doping level close to that of the $La_4Ni_3O_8$ samples from Ref. [21], where a clear pre-peak at 530 eV was observed. A very small spectral weight gain is also observed in our O-*K* data, however much smaller than the additional weight above 531 eV. Hence we conclude that a partial oxygen reduction of infinite-layer nickelate films causes a different modification of the electronic structure than the one realized in the $La_4Ni_3O_8$ single crystals. A possible explanation could be a Hund's

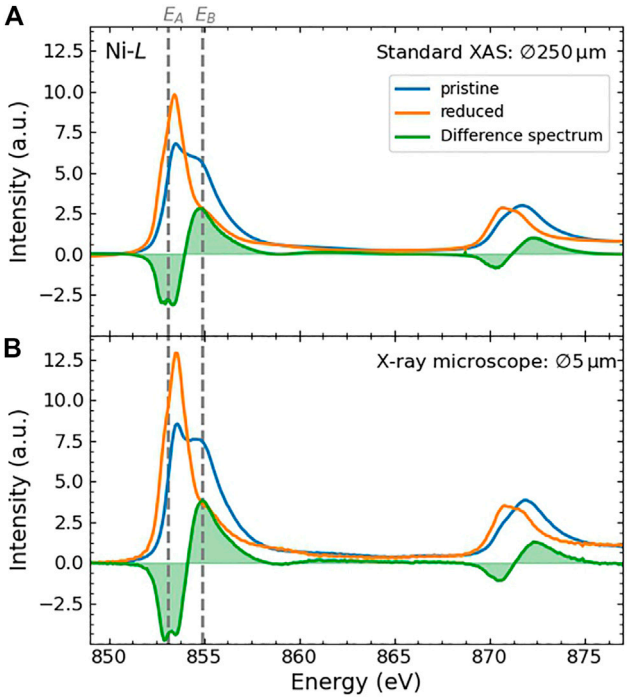

FIGURE 2 | XAS measurements across the Ni *L*-edge from a pristine and reduced $PrNiO_3$ thin film in a standard experimental setup **(A)** and with an x-ray microscope **(B)**. The latter measurement agrees well with XAS measured using a much larger beam, shown in panel **(A)**. From the difference spectrum (green curve), we extract two energies E_A = 853.1 eV and E_B = 854.9 eV, where the contrast between pristine and reduced is the largest. The two energies are indicated by gray dashed lines. Subsequently, we take image scans with varying size/resolution at peak A and B on the reduced sample to check for possible oxygen inhomogeneities (see **Figure 4**).

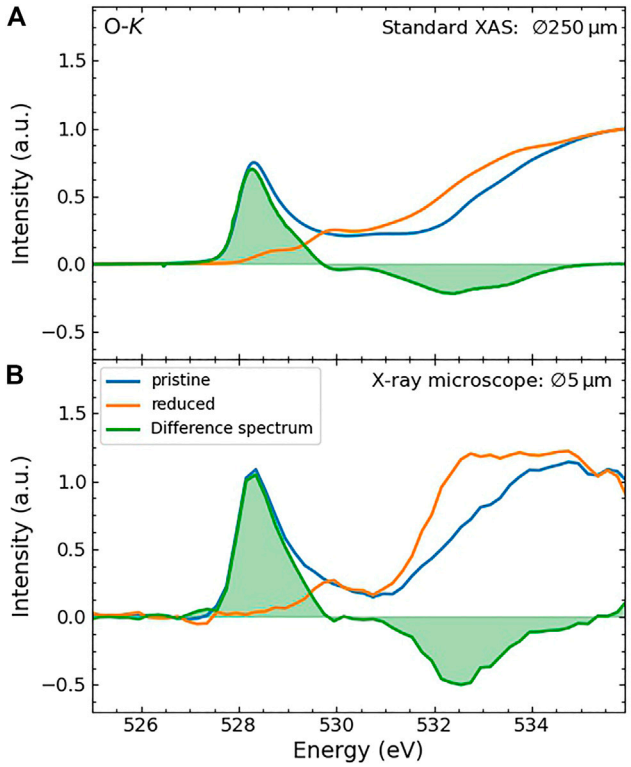

FIGURE 3 | Oxygen *K*-edge XAS measurements for both the pristine and reduced $PrNiO_3$ thin film in a standard experimental setup **(A)** and at the x-ray microscope **(B)**. The spectral weight around 528 eV ("pre-peak") vanishes upon reduction, in agreement with previous studies.

coupling stabilized trapping of holes at sites with a remaining apical oxygen, similar to what was inferred for layer-selective reduced $LaNiO_{2+\delta}$-$LaGaO_3$ superlattices [16].

3.2 X-Ray Microscopy

We now move to a detailed investigation of the lateral distribution of oxygen inhomogeneity in the reduced $PrNiO_{2+\delta}$ films and the associated Ni 3*d* state filling. To this end we exploit the unprecedented capabilities of an x-ray microscope such as MAXYMUS to spatially resolve features with a resolution down to 50 nm. We studied the spatial distribution of the oxygen content using image scans, *i.e.* the incident energy is fixed while we record the TEY signal at different locations across the sample. Since the absorption signal and consequently the corresponding (absolute) contrast, is much higher at the Ni-*L* edge, we use the Ni-L_3 edge for our spatially resolved study, instead of the O-*K* edge. To maximize sensitivity to potential inhomogenieties, we choose the energies for the subsequent mapping to be at the maximum difference between the reduced and pristine sample (see **Figure 2**, green line). Following this procedure, we identify two energies: peak *A* at E_A = 853.1 eV and peak *B* at E_B = 854.9 eV, which are indicated with dashed gray lines in **Figure 2**.

We performed several image scans with varying spatial resolution and incident energies E_A and E_B as shown in the upper row of **Figure 4**. In the image scans with different lateral resolution, we find similar intensities across the investigated sample region, which indicates a spatially homogeneous Ni valence and the associated homogeneity of the oxygen distribution. Additionally we show the difference image for the two images taken at peak *A* and *B*. We emphasize that for possibly unreduced sample areas, we would expect a negative contrast (dark red in the chosen colour scheme). As can be seen from the difference image, we do not identify such contrast regions and hence conclude at the length scale investigated here (> 50 nm) the oxygen stoichiometry is laterally constant. This observation is further supported by analysing the image scans using histrograms (lower row of the corresponding **Figure 4**). Here, we group the pixels according to their intensity and subsequently show the number of pixels versus the normalized intensity. This representation illustrates that the intensity is evenly distributed around the value expected for a fully and homogeneously reduced sample.

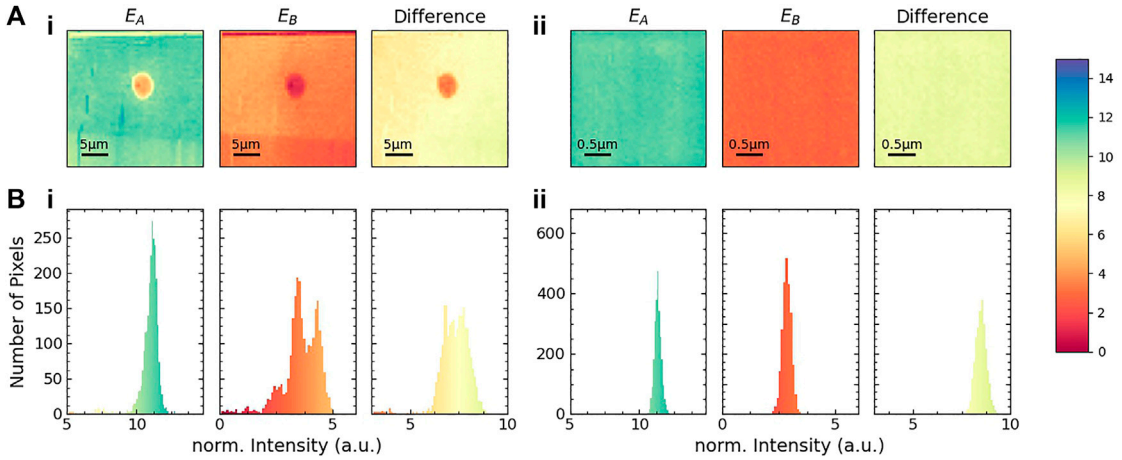

FIGURE 4 | Spatially resolved XAS measurements of the $PrNiO_{2+\delta}$ thin film. *upper row:* Image scans at peak A, peak B, and the difference image: A—B for two different image, and corresponding pixel sizes. The images on the left (right) have a lateral size of 25 μm × 25 μm (2.5 μm × 2.5 μm). This corresponds to a resolution, *i.e.*, pixel size, of 500 and 50 nm for left and right panels, respectively. The colorbar on the right side gives the normalized intensity for all image scans. **(Bi, Bii)***:* Histograms of the images shown in the **(Ai, Aii)**. For both image sizes, the intensity distribution is centered around the TEY value from the energy scan (**Figure 2**) of the reduced film. Note that all scans (image and energy scans) were taken in TEY mode at room temperature. The artifact (dot-like structure) in the larger images (upper left) probably results from surface contamination or surface defects, lowering the overall XAS intensity of the underlying sample. We emphasize that this is a region of reduced XAS signal, and can in particular not be identified as an unreduced patch, which would appear in dark red in the difference image and brighter than the background in the E_B image.

4 DISCUSSION

Due to a lack of studies on the lateral, spatially resolved properties of the infinite-layer nickelates[1], we compare and relate our x-ray microscopy study to similar experiments on other perovskite compounds, including the RNiO$_3$. In particular, we focus on photo-emission electron microscopy (PEEM) and magnetic resonant elastic x-ray scattering (REXS) to review the spatial distribution of different characteristics, such as the metal-to-insulator transition and magnetic domain structures.

In the following paragraphs, we illustrate that our study allows to rule out lateral inhomogeneities with length scales similar to those observed in other related oxide compounds. Several PEEM studies investigate the spatial variation of different characteristics in $SrTiO_3$, a prototypical and widely studied oxide material. Ferromagnetic domains, randomly distributed in $SrTiO_3$, have a typical size of approx. 40 nm at room temperature [27]. Further, domains in the $SrTiO_3$ surface polarization [28] originating from local defects, studied with PEEM using a 400 nm-sized beam revealed polarized regions with sizes of several μm. Consequently, we argue that possible spatial variations of our reduced samples within these typical length scales should have been visible in our study, and hence this points again towards a laterally homogeneous topotactical reduction.

A spatially resolved study of the metal-to-insulator transition (MIT) in $NdNiO_3$ epitaxial thin films was carried out by Mattoni *et al.* [29]. The authors use PEEM with a resolution of a few tens of nm, which is very comparable to our x-ray microscopy study. The PEEM contrast results from the difference of the XAS spectra for metallic and insulating regions and can be quantified as the ratio of the difference between metallic and insulating regions to the XAS intensity at a specific energy, resulting in a maximal PEEM contrast at the Ni-L_3 edge of approx. 1%. This contrast is enough to map the evolution and nucleation of metallic/insulating domains upon warming/cooling and to identify structures of approx. 250 nm (smaller length scale of the structure). Comparing the PEEM contrast of this study to our x-ray microscopy experiment [c.f. **Figure 2**, ratio of difference spectrum (green line) to XAS intensity (orange) at peak A of the reduced sample], we expect a contrast of approx. 50% , thereby more than one order of magnitude higher. We therefore conclude, that variations on similar length scales as those of locally distinct T_{MIT} would have been visible in our experiment, if present.

Comparing our results with the study of magnetic domains in $NdNiO_3$ using nanoprobe magnetic scattering of the characteristic antiferromagnetic (AFM) peak, which reveals magnetic textures with sizes of several hundred nm up to 250 μm [30]. The lateral resolution of this study is 100 nm and hence very comparable to our investigation. While the magnetic structure in the perovskite phase seems to be modulated within length scales of hundreds of nm, we do not find any indications of variation in the oxygen content at a similar length scale.

Finally, we compare our x-ray microscopy study to available scanning transmission electron microscopy measurements on nickelates. In particular, STEM-EELS constitutes a

[1]To the best of our knowledge, Ref. [26] is the only available spatially resolved study comparing layered and perovskite oxides. The authors use electrochemical strain microscopy to investigate surfaces of Co-based compounds with a resolution of 10 nm and reveal electrochemical activity on the length scales of approx. 50 to 100 nm.

complementary method to map out the chemical composition of oxide materials within atomic resolution. Superconducting Sr-doped $NdNiO_2$ thin films have been studied with STEM, indicating defects, primarily resulting from stacking faults of the Ruddlesden-Popper-type [3, 15]. However, a detailed investigation of the oxygen positions, including potential variations of the reduction state, is still lacking in thin film compounds. A comprehensive STEM-EELS characterization of infinite-layer $La_{1-x}Ca_xNiO_{2+\delta}$ single crystals indicates that some apical oxygen atoms remain after the topotactic reduction [31]. This suggests that the soft chemistry reduction process might be non-homogeneous on the length scale of single atoms, while still most parts of the sample transition to the infinite-layer phase. Atomic resolution is beyond the capabilities of our x-ray microscope. We emphasize that despite the somewhat better spatial resolution in STEM studies, x-ray microscopy has the advantage of being a destruction-free method. Additionally, the samples are easy to prepare (if we consider the TEY mode that is used in our study), and in particular several etching and milling processes, which are necessary for STEM specimen preparation, can be avoided, thereby maintaining the sensitive oxygen stoichiometry.

5 SUMMARY

In summary, we used total electron yield XAS both in a standard experimental configuration and in an x-ray microscope to probe topotactically reduced $PrNiO_{2+\delta}$. We confirm a spatially homogeneous oxidation state within the length scales probed in our experiment (resolution approx. 50 nm). Consequently, we conclude that the oxygen de-intercalation processes upon soft-chemistry reduction from the perovskite precursor to infinite-layer phase occurs homogeneously across the sample. Our study illustrates the power of non-destructive spatially-resolved XAS measured in an x-ray microscope to confirm lateral homogeneity in correlated oxide materials. In the future it would be interesting to study the depth-depended oxidation profiles to investigate possible differences in the reduction of layers next to the surface or interface and the inner layers in infinite layer nickelates.

DATA AVAILABILITY STATEMENT

The raw data supporting the conclusions of this article will be made available by the authors, without undue reservation.

AUTHOR CONTRIBUTIONS

EB, KF, and MB conceived the project. The samples were grown, reduced, and characterized by RP, where RO provided guidance on the reduction procedure. The spatially resolved data was taken by KF, SW, and MW with remote support from MB and RP. The standard XAS measurements were performed by KF, RP and ES. KF performed the data analysis. KF and EB wrote the manuscript with input from all co-authors. GS, BK, and EB coordinated the project.

FUNDING

We acknowledge financial support by the Center for Integrated Quantum Science and Technology (IQ^{ST}) and the Deutsche Forschungsgemeinschaft (DFG, German Research Foundation): Projektnummer 107745057—TRR 80.

ACKNOWLEDGMENTS

We thank HZB for the allocation of synchrotron radiation beamtime.

REFERENCES

1. Anisimov VI, Bukhvalov D, Rice TM. Electronic Structure of Possible Nickelate Analogs to the Cuprates. *Phys Rev B* (1999) 59:7901–6. doi:10.1103/PhysRevB.59.7901
2. Li D, Lee K, Wang BY, Osada M, Crossley S, Lee HR, et al. Superconductivity in an Infinite-Layer Nickelate. *Nature* (2019) 572:624–7. doi:10.1038/s41586-019-1496-5
3. Li D, Wang BY, Lee K, Harvey SP, Osada M, Goodge BH, et al. Superconducting Dome in $Nd_{1-x}Sr_xNiO_2$ Infinite Layer Films. *Phys Rev Lett* (2020) 125:027001. doi:10.1103/PhysRevLett.125.027001
4. Zeng S, Tang CS, Yin X, Li C, Li M, Huang Z, et al. Phase Diagram and Superconducting Dome of Infinite-Layer $Nd_{1-x}Sr_xNiO_2$ Thin Films. *Phys Rev Lett* (2020) 125:147003. doi:10.1103/PhysRevLett.125.147003
5. Osada M, Wang BY, Lee K, Li D, Hwang HY. Phase Diagram of Infinite Layer Praseodymium Nickelate Pr1−$_{xSr}$xN$_i$O2 $_T$hin Films. *Phys .Rev .Mater* (2020) 4: 121801. doi:10.1103/PhysRevMaterials.4.121801
6. Zeng SW, Yin XM, Li CJ, Tang CS, Han K, Huang Z, et al. *Observation of Perfect Diamagnetism and Interfacial Effect on the Electronic Structures in nd0.8sr0.2nio2 Superconducting Infinite Layers* (2021). arXiv:2104.14195.
7. Zhang Y, Lin LF, Hu W, Moreo A, Dong S, Dagotto E. Similarities and Differences between Nickelate and Cuprate Films Grown on a $Srtio_3$ Substrate. *Phys Rev B* (2020) 102:195117. doi:10.1103/PhysRevB.102.195117
8. Lee KW, Pickett WE. Infinite-layer $LaNio_2$: Ni^{1+} Is Not Cu^{2+}. *Phys Rev B* (2004) 70:165109. doi:10.1103/PhysRevB.70.165109
9. Botana AS, Norman MR. Similarities and Differences between $Lanio_2$ and $Cacuo_2$ and Implications for Superconductivity. *Phys Rev X* (2020) 10:011024. doi:10.1103/PhysRevX.10.011024
10. Pan GA, Segedin DF, LaBollita H, Song Q, Nica EM, Goodge BH, et al. Superconductivity in a Quintuple-Layer Square-Planar Nickelate. *Nat. Mater.* (2021). doi:10.1038/s41563-021-01142-9
11. Rossi M, Lu H, Nag A, Li D, Osada M, Lee K, et al. Orbital and Spin Character of Doped Carriers in Infinite-Layer Nickelates. *Phys. Rev. B* (2020) 104(22): L220505. doi:10.1103/PhysRevB.104.L220505
12. Lu H, Rossi M, Nag A, Osada M, Li DF, Lee K, et al. Magnetic Excitations in Infinite-Layer Nickelates. *Science* (2021) 373:213–6. doi:10.1126/science.abd7726
13. Katukuri VM, Bogdanov NA, Weser O, van den Brink J, Alavi A. Electronic Correlations and Magnetic Interactions in Infinite-Layer $NdNiO_2$. *Phys Rev B* (2020) 102:241112. doi:10.1103/PhysRevB.102.241112

14. Hepting M, Li D, Jia CJ, Lu H, Paris E, Tseng Y, et al. Electronic Structure of the Parent Compound of Superconducting Infinite-Layer Nickelates. *Nat Mater* (2020) 19:381–5. doi:10.1038/s41563-019-0585-z
15. Goodge BH, Li D, Lee K, Osada M, Wang BY, Sawatzky GA, et al. Doping Evolution of the mott–hubbard Landscape in Infinite-Layer Nickelates. *Proc Natl Acad Sci* (2021) 118.
16. Ortiz RA, Menke H, Misják F, Mantadakis DT, Fürsich K, Schierle E, et al. Superlattice Approach to Doping Infinite-Layer Nickelates. *Phys Rev B* (2021) 104:165137. doi:10.1103/PhysRevB.104.165137
17. Chen CT, Tjeng LH, Kwo J, Kao HL, Rudolf P, Sette F, et al. Out-of-plane orbital characters of intrinsic and doped holes in $la_{2-x}sr_xcuo_4$. *Phys Rev Lett* (1992) 68:2543–6. doi:10.1103/PhysRevLett.68.2543
18. Lee K, Goodge BH, Li D, Osada M, Wang BY, Cui Y, et al. Aspects of the Synthesis of Thin Film Superconducting Infinite-Layer Nickelates. *APL Mater* (2020) 8:041107. doi:10.1063/5.0005103
19. Li J, Green RJ, Zhang Z, Sutarto R, Sadowski JT, Zhu Z, et al. Sudden Collapse of Magnetic Order in Oxygen-Deficient Nickelate Films. *Phys Rev Lett* (2021) 126:187602. doi:10.1103/PhysRevLett.126.187602
20. Abbate M, Zampieri G, Prado F, Caneiro A, Gonzalez-Calbet JM, Vallet-Regi M. Electronic Structure and Metal-Insulator Transition in $Lanio_{3-\delta}$. *Phys Rev B* (2002) 65:155101. doi:10.1103/PhysRevB.65.155101
21. Lin JQ, Villar Arribi P, Fabbris G, Botana AS, Meyers D, Miao H, et al. Strong Superexchange in a $D^{9-\delta}$ Nickelate Revealed by Resonant Inelastic X-ray Scattering. *Phys Rev Lett* (2021) 126:087001. doi:10.1103/PhysRevLett.126.087001
22. Weigand M. *Realization of a New Magnetic Scanning X-ray Microscope and Investigation of Landau Structures under Pulsed Field Excitation*. Göttingen: Cuvillier Verlag (2015).
23. Green RJ, Haverkort MW, Sawatzky GA. Bond Disproportionation and Dynamical Charge Fluctuations in the Perovskite Rare-Earth Nickelates. *Phys Rev B* (2016) 94:195127. doi:10.1103/PhysRevB.94.195127
24. Medarde M, Dallera C, Grioni M, Delley B, Vernay F, Mesot J, et al. Charge Disproportionation in $Rnio_3$ Perovskites (R=rare Earth) from High-Resolution X-ray Absorption Spectroscopy. *Phys Rev B* (2009) 80:245105. doi:10.1103/PhysRevB.80.245105
25. Fürsich K, Lu Y, Betto D, Bluschke M, Porras J, Schierle E, et al. Resonant Inelastic X-ray Scattering Study of Bond Order and Spin Excitations in Nickelate Thin-Film Structures. *Phys Rev B* (2019) 99:165124. doi:10.1103/PhysRevB.99.165124
26. Kumar A, Leonard D, Jesse S, Ciucci F, Eliseev EA, Morozovska AN, et al. Spatially Resolved Mapping of Oxygen Reduction/evolution Reaction on Solid-Oxide Fuel Cell Cathodes with Sub-10 Nm Resolution. *ACS Nano* (2013) 7:3808–14. doi:10.1021/nn303239e
27. Taniuchi T, Motoyui Y, Morozumi K, Rödel TC, Fortuna F, Santander-Syro AF, et al. Imaging of Room-Temperature Ferromagnetic Nano-Domains at the Surface of a Non-magnetic Oxide. *Nat Commun* (2016) 7:11781. doi:10.1038/ncomms11781
28. Chen J, Liu W, Eul T, Chen M, Hu X, Wang S, et al. Engineering of Electron Confinement through Defect-Based Localized Polarization on Srtio3 Surface. *Adv Electron Mater* (2021) 7:2000968. doi:10.1002/aelm.202000968
29. Mattoni G, Zubko P, Maccherozzi F, van der Torren AJH, Boltje DB, Hadjimichael M, et al. Striped Nanoscale Phase Separation at the Metal–Insulator Transition of Heteroepitaxial Nickelates. *Nat Commun* (2016) 7:13141. doi:10.1038/ncomms13141
30. Li J, Pelliciari J, Mazzoli C, Catalano S, Simmons F, Sadowski JT, et al. Scale-invariant Magnetic Textures in the Strongly Correlated Oxide Ndnio3. *Nat Commun* (2019) 10:4568. doi:10.1038/s41467-019-12502-0
31. Puphal P, Wu YM, Fürsich K, Lee H, Pakdaman M, Bruin JAN, et al. *Synthesis and Characterization of Ca-Substituted Infinite-Layer Nickelate Crystals*. arXiv: 2106 (2021). p. 13171.

Conflict of Interest: The authors declare that the research was conducted in the absence of any commercial or financial relationships that could be construed as a potential conflict of interest.